Journal of the Korean Physical Society, Vol. 62, No. 1, January 2013, pp. 67∼72

Effects of Gas Flow Rate on the Etch Characteristics of a Low-k SiCOH Film with an Amorphous Carbon Mask in Dual-frequency $CF_4/C_4F_8/Ar$ Capacitively-coupled Plasmas

Bong-Soo Kwon and Hea-Lim Lee
Department of Advanced Materials Science & Engineering, Sungkyunkwan University, Suwon 440-746, Korea

Nae-Eung Lee*
SKKU Advanced Institute of Nanotechnology (SAINT), Sungkyunkwan University, Suwon 440-746, Korea

Chang-Young Kim and Chi Kyu Choi
Nano Thin Film Materials Laboratory, Department of Physics and Research Institute for Basic Sciences, Jeju National University, Jeju 690-756, Korea

(Received 5 October 2012, in final form 9 November 2012)

Highly selective nanoscale etching of a low-dielectric constant (low-k) organosilicate (SiCOH) layer using a mask pattern of chemical-vapor-deposited (CVD) amorphous carbon layer (ACL) was carried out in $CF_4/C_4F_8/Ar$ dual-frequency superimposed capacitively-coupled plasmas. The etching characteristics of the SiCOH layers, such as the etch rate, etch selectivity, critical dimension (CD), and line edge roughness (LER) during the plasma etching, were investigated by varying the C_4F_8 flow rate. The C_4F_8 gas flow rate primarily was found to control the degree of polymerization and to cause variations in the selectivity, CD and LER of the patterned SiCOH layer. Process windows for ultra-high etch selectivity of the SiCOH layer to the CVD ACL are formed due to the disproportionate degrees of polymerization on the SiCOH and the ACL surfaces.

PACS numbers: 52.77.Bn, 85.40.Hp
Keywords: ACL, Organosilicate glasses (SiCOH), Etch selectivity, Line edge roughness (LER), Plasma etching, Dual-frequency superimposed capacitively-coupled plasma (DFS-CCP)
DOI: 10.3938/jkps.62.67

I. INTRODUCTION

The critical dimension (CD) of the features in ultra-large-scale integrated (ULSI) circuits continues to decrease in the frame of three-dimensional multilayer interconnects. The decreasing feature size in multilayer interconnects primarily causes an increase in the RC (resistance-capacitance) delay. For increased performance of a highly-integrated Si chip, one solution for reducing the RC delay is to replace conventional Al wires with low-resistivity Cu and to introduce new materials with dielectric constants lower than that of traditional silicon dioxide (SiO_2) [1–3]. For integration of the Cu interconnect, a dual damascene, based on plasma etching of low-dielectric-constant (low-k) dielectrics such as organosilicate (SiCOH) layers, and Cu gap-filling process is the key technology [4].

If nano-scale patterns of low-k dielectric materials are to be created, a multi-layer resist (MLR) structure is used due to difficulty in directly patterning the low-k dielectrics with a photoresist (PR) mask. A typical multilayer resist (MLR) structure is composed of silicon oxide (SiO_2), a silicon-nitride (Si_3N_4) or a silicon-oxynitride (SiON) hardmask, an amorphous carbon layer (ACL), and a dielectric underlayer. Etch processes for the SiO_2, Si_3N_4 and SiON hard-mask using a 193 nm ArF photoresist are critically important during patterning of MLR structures due to the continuously decreasing resist thickness [5]. The line edge roughness (LER) and the critical dimension (CD) have also become important issues in patterning nano-scale features because the LER and the CD of the hard-mask patterns are transferred to the ACL and the underlayer during dry etching [6,7]. For precise patterning of the underlayer in the MLR structure, therefore, understanding the LER and the CD variations in the ACL and the final underlayer during dry etching is important.

During etching of the underlayers using an ACL mask for sub-50-nm nano-scale patterning, a very high

*E-mail: nelee@skku.edu; Tel: +82-31-290-7398; Fax: +82-31-290-7410

aspect ratio of the ACL/underlayer etch structure is expected due to the relatively thick chemical-vapor-deposited (CVD) ACL that is used with current state-of-the-art patterning technology. Furthermore, highly selective etching of the SiCOH underlayer in F-containing etch environments by using a CVD ACL etch mask is expected to be very difficult due to the relatively low etch resistance of the CVD ACL. If the ease of profile control during etching, is to be increased highly selective etch processes with a thinner CVD ACL mask that in reduce of the aspect ratio of the etch structures are expected to be very useful.

In this study, we investigated the possibility of obtaining a highly selective etching process of SiCOH by using a CVD ACL mask in the MLR structure of ArF PR/bottom anti-reflective coating (BARC)/SiO_x/CVD ACL/SiCOH in a CF_4/C_4F_8/Ar dual-frequency superimposed capacitively-coupled plasma (DFS-CCP). We also studied the variations of the LER and CD of SiCOH etched with the CVD ACL mask pattern by varying the C_4F_8 gas flow, which is a critical process parameter. The ability to obtain an ultra-high etch selectivity of the SiCOH layer to the ACL etch mask was confirmed for a narrow process window.

II. EXPERIMENTAL

An eight-inch DFS-CCP dielectric etcher was used for the etching experiments. A schematic of the DFS-CCP etch system used in the present experiment has been shown elsewhere [8,9]. The system was equipped with three different HF (high-frequency) power sources (13.56, 27.12, and 60 MHz) and a LF (low-frequency) power source (2 MHz). Throughout the experiments in this work, HF and LF source frequencies of 27.12 and 2 MHz were used, respectively. The HF power source controls the plasma generation, *i.e.*, the fluxes and the species of the ions and the radicals, while the LF power source controls the dynamics of the ions in the sheath where the degree of ion acceleration, *i.e.*, ion energy, is controlled [10–13].

To apply CVD ACL as an etch mask for SiCOH etching, we prepared wafers with patterns of ArF PR with a thickness of 150 nmon a stack of BARC (∼30 nm)/SiO_x (∼50 nm)/CVD ACL (∼300 nm)/SiCOH (≥600 nm)/ Si (001) by photolithographic patterning using an ArF scanner. The critical dimension (CD) of the ArF line pattern used in this work was ∼215 nm. After the ACL had been patterned, the space opening and the linewidth of the ACL as the final hard mask were around 150 nm and 197 nm, respectively.

Etching experiments were carried out in the following sequential order: ArF PR, BARC, SiO_x hard mask, CVD ACL, and SiCOH underlayer. The BARC layer was etched in a CF_4 (35 SCCM)/O_2 (5 SCCM)/Ar (300 SCCM) plasma for 40 seconds with HF source power (P_{HF}), LF source power (P_{LF}), HF source frequency (f_{HF}), and LF source frequency (f_{LF}) values of 300 W, 100 W, 27.12 MHz, and 2 MHz, respectively. This was followed by SiO_x hard-mask etching in a C_4F_8 (20 SCCM)/CH_2F_2 (15 SCCM)/O_2 (15 SCCM)/Ar (300 SCCM) plasma for 50 s with P_{HF}, P_{LF}, f_{HF}, and f_{LF} values of 600 W, 300 W, 27.12 MHz, and 2 MHz, respectively. The CVD ACL was etched in an O_2 (400 SCCM)/N_2 (50 SCCM)/Ar (200 SCCM) plasma for 50 s with P_{HF}, P_{LF}, f_{HF}, and f_{LF} values of 600 W, 300 W, 27.12 MHz, and 2 MHz, respectively. A CF_4/C_4F_8/Ar gas mixture was used to etch the final SiCOH layer because C_4F_8 gas is a highly polymerizing etch gas that allows the degree of polymerization on the ACL to be tuned. During etching of the SiCOH layer throughout the experiments, the chamber pressure, CF_4 flow rate, and Ar flow rates were kept at 230 mTorr, 50 SCCM, and 300 SCCM, respectively.

The etch rate and the profile of the patterned ArF PR/BARC/SiO_x/ACL/SICOH stack were measured using a field emission scanning electron microscope (FE-SEM, JEOL JSM-7500F). The LER of the stacked structure before and after etching was analyzed using SEM Metrology Interactive Toolbox (SUMMIT) software (EUV Technology). The chemical information for the CVD ACL and SiCOH layer surfaces etched under different etching parameters was determined from the C 1*s* and the F 1*s*spectra recorded by using X-ray photoelectron spectroscopy (XPS). The Mg Kα source for XPS emits a non-monochromatic X-ray at 1253.6 eV. XPS narrow scan spectra from all the interesting regions were recorded with a pass energy of 20 eV in order to qualitatively identify the chemical binding states. A take-off angle (*i.e.*, the angle between the axis of the detector and the sample surface) of 90° was used for the XPS measurements.

III. RESULTS AND DISCUSSION

The effects of C_4F_8 flow rate on the etch rates of the ACL and the SiCOH layers and on the etch selectivity during SiCOH etching using the ACL mask were first investigated by varying the C_4F_8 flow rate in the CF_4/C_4F_8/Ar chemistry at a fixed f_{HF} of 27.12 MHz and a f_{LF} of 2 MHz. During these experiments, the P_{HF}, P_{LF}, and etch time were kept at 600 W, 300 W, and one minute, respectively. Figure 1 shows the etch rates of the CVD ACL and the SiCOH layers and the etch rate selectivity as the C_4F_8 flow rate was varied from 0 to 30 SCCM. Increasing the C_4F_8 flow rate was very effective in enhancing the etch selectivity due to the resulting significant decrease in the etch rate of the ACL and the slight decrease in the SiCOH etch rate in the C_4F_8 flow rate range of 0 to 30 SCCM, as shown in Fig. 1. At C_4F_8 flow rates greater than 10 SCCM, the ACL was not etched, which indicates deposition of

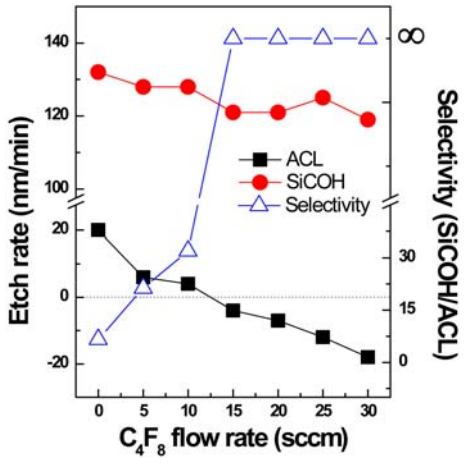

Fig. 1. (Color online) Etch rates of the SiCOH and the CVD ACL etched for one minute under the condition of P_{HF} (600 W)/P_{LF} (300 W)/230 mTorr/CF_4 (50)/C_4F_8 (varied)/300 Ar.

a hydrofluorocarbon (CH_xF_y) layer on the ACL. Due to the differential etch characteristics of the two layers, an ultra-high etch selectivity of the SiCOH/ACL was obtained at C_4F_8 flow rates greater than 10 SCCM.

To investigate the variations in the CD size (nm) and the LER (3σ) of SiCOH /ACL pattern etched in CF_4 (50)/C_4F_8(varied)/Ar (300) plasmas, we measured the CD size (nm) and the LER (3σ) values before etching and after each etch step by varying the C_4F_8 flow rates from 0 to 30 SCCM, as shown in Fig. 2. The CD size (nm) and the LER (3σ) values in Figs. 2(a) and 2(b), respectively, were also obtained from samples etched by varying the C_4F_8 flow rates from 0 to 30 SCCM. Before etching, the average CD size (nm) and LER (3σ) of unetched SiCOH with the patterned ACL mask were 214 and 2.1 nm, respectively. The CD size and the LER values tended to decrease with BARC open, SiO_x etch, and ACL etch in sequence. However, the CD size and the LER values tended to increase when the C_4F_8 flow rate was increased slightly during SiCOH etching, as shown in Figs. 2(a) and 2(b).

In order to understand the variations in the etch selectivity, CD and LER during SiCOH etching, were used XPS to examined the chemical binding states and composition of the SiCOH and the ACL surfaces etched under different C_4F_8 flow rates. Figures 3(a) – 4(d) show the C 1s, F 1s, O 1s, and Si 2p spectra, respectively, obtained from the SiCOH layer etched with different C_4F_8 flow rates. The peaks corresponding to the C-C or the C-H bonds, the C-CF_x bonds, and the CF_x (x = 1, 2) groups are assigned in the C 1s spectra in Fig. 4(a). The peak corresponding to the C-C or the C-H bonds was assigned at a binding energy (BE) of 285 eV [14,15]. The C-CF_x peaks at a BE of 287.6 eV are attributed to the non-functionalized sp^2 C or sp^3 C in the β position of two or three F atoms (not directly bound to F atoms),

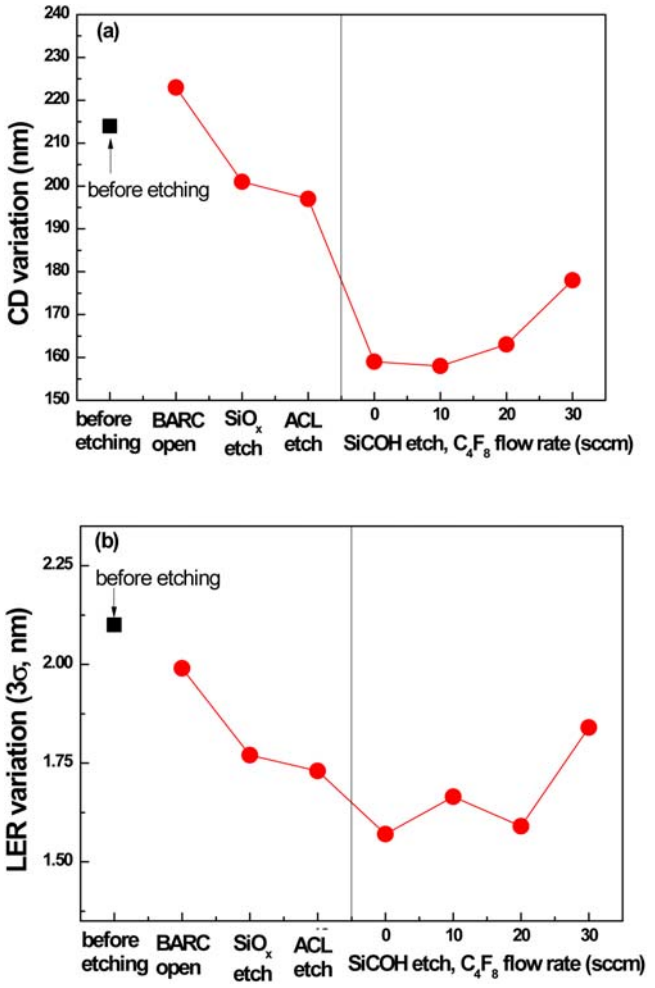

Fig. 2. (Color online) Variation of the (a) CD size (nm) and the (b) LER (3σ) of the etched patterns during each etch step.

respectively [14,15]. The peaks corresponding to CF due to the covalent bonding of C with F in the CF group are assigned at BEs that are shifted 5.2 eV from the C-C peak [14,15]. The C 1s and the F 1s spectra in Fig. 3 indicate that a thin steady-state CH_xF_y layer containing mainly C-C, C-H, and C-CF_x bonds was formed on the SiCOH. As the C_4F_8 flow rate was increased from 0 to 20 SCCM, the intensities of the C-CF_x, CF, and CF_2 peaks decreased. At a C_4F_8 flow rate of 30 SCCM, however, the intensities of the C 1s peaks increased quickly due to the deposition of a thicker CH_xF_y layer.

The F 1s spectra in Fig. 3(b) show CF_x peaks corresponding to a BE of 687.1 eV. The CF_x peak at a BE of 687.1 eV represents the same component as the CF and the CF_2 peaks because the chemical shift of the F 1s core level does not depend on the x value of the CF_x group [15]. The peak intensity of the F 1s spectrum did not change significantly with increasing a C_4F_8 flow rate from 0 to 20 SCCM and then rapidly increased at a C_4F_8 flow rate of 30 SCCM, which indicates the deposition of

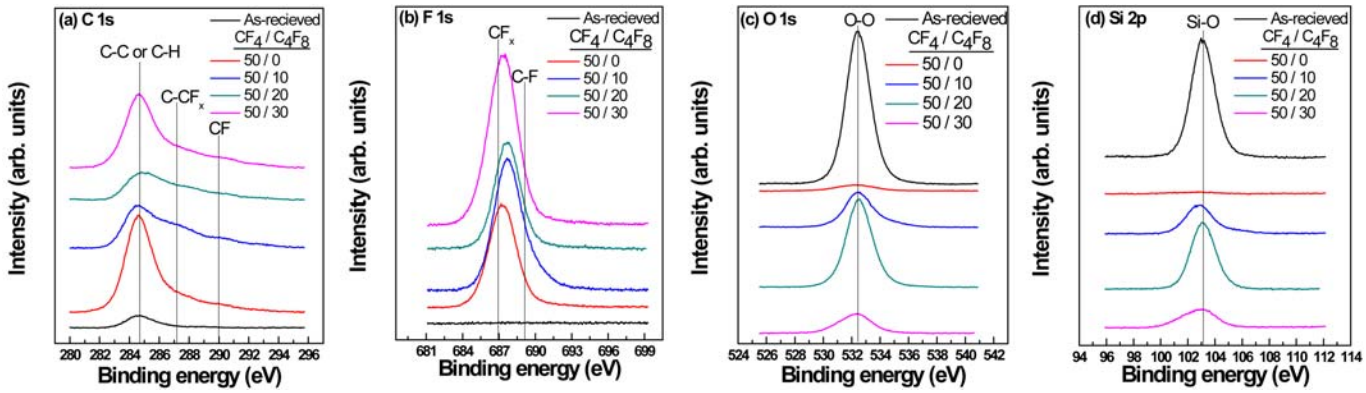

Fig. 3. (Color online) XPS spectra obtained from the etched blanket SiCOH layer: (a) C 1s, (b) F 1s, (c) O 1s, and (d) Si 2p. The samples were etched for one minute under the condition of P_{HF} (600 W)/P_{LF} (300 W)/230 mTorr/CF_4 (50 SCCM)/C_4F_8 (varied)/300 Ar.

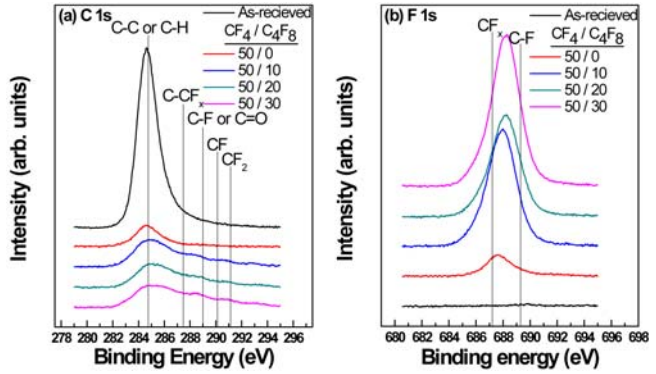

Fig. 4. (Color online) XPS spectra obtained from the etched blanket CVD ACL: (a) C 1s and (b) F 1s. The samples were etched for one minute under the condition of P_{HF} (600 W)/P_{LF} (300 W)/230 mTorr/CF_4 (50 SCCM)/C_4F_8 (varied)/300 Ar.

a thicker CH_xF_y layer on the SiCOH surface at a C_4F_8 flow rate of 30 SCCM.

The O 1s and the Si 2p spectra are shown in Figs. 3(c) and 3(d), respectively. With no C_4F_8 flow, C and Si elements are depleted on the surface of the SiCOH layer. As the C_4F_8 flow rate was increased to 20 SCCM, the peak intensities of the O 1s and the Si 2p spectra increased, presumably due to the lack of any dramatic change in the steady-state polymer thickness. At a C_4F_8 flow rate of 30 SCCM, the O 1s and the Si 2p peak intensities decreased quickly, presumably due to the formation of a thicker polymer layer.

The C 1s and the F 1s XPS spectra obtained from the etched CVD ACLs were also measured in order to compare them with those of etched SiCOH layers. Figures 4(a) and 4(b) show the C 1s and the F 1s spectra, respectively, obtained from the etched CVD ACL at various C_4F_8 flow rates. The etching conditions were the same as those used to obtain the data in Fig. 1. The BE assignments of the C-C, C-CF_x, CF, and CF_2 peaks are the same as there of the C 1s spectra obtained from the etched silicon oxide. The intensity of the C-C or the C-H peaks from the CVD ACL gradually decreased with increasing C_4F_8 flow rate, but the C-CF_x, CF, and CF_2 peak intensities were increased with increasing C_4F_8 flow rate, which indicates the deposition of a CH_xF_y layer with a higher F content. The F 1s spectra in Fig. 4(b) show the peaks corresponding to BEs of 687.1 eV. The peak intensity of the F 1s spectra gradually increased with increasing C_4F_8 flow rate. These results also indicate the deposition of a CH_xF_y layer with increasing F content.

From the XPS spectra in Figs. 4 and 5, the F/C ratio was obtained to better understand the effects of the C_4F_8 flow rate on the characteristics of the steady-state CH_xF_y layers on the etched ACL and SiCOH surfaces, which are shown in Figs. 5(a) and 5(b), respectively. The Si/O ratio of the etched SiCOH surfaces was also obtained, and the results are shown in Fig. 5(c). The F/C and the Si/O ratios were calculated from the total integrated area of the high-resolution XPS spectra by considering sensitivity factors of 1, 0.296, 0.283, and 0.711 for fluorine, carbon, silicon, and oxygen, respectively [16].

As shown in Fig. 5(a), the F/C ratio of the etched ACL surface gradually increased with increasing C_4F_8 flow rate due to the deposition of a CH_xF_y layer with increasing F content. The observed increase in the F/C ratio of the ACL surface with increasing C_4F_8 flow rate is probably attributed to the increased density of F-containing radicals in the plasma. The F/C ratio on the SiCOH layer increased as the C_4F_8 flow rate was increased from 0 to 20 SCCM and then decreased slightly (Fig. 5(b)). The formation of a CH_xF_y layer with increasing F content as the C_4F_8 flow rate increased might facilitate the etching reaction, leading to a slight decrease in the SiCOH etch rate (Fig. 1). At a C_4F_8 flow rate of 30 SCCM, the F/C ratio was slightly decreased, presumably due to the C-rich polymer caused by reduced consumption of carbon in the CH_xF_y layer. Interestingly, the F/C ratios on the SiCOH surface were smaller than those on the ACL sur-

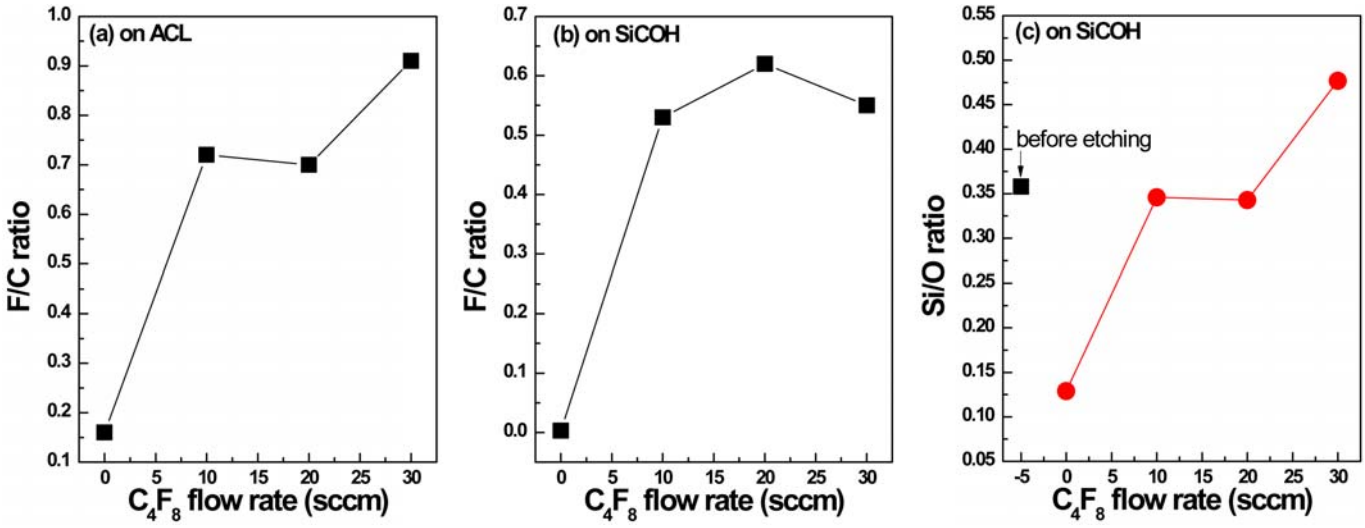

Fig. 5. (Color online) Composition variation of etched surfaces with various C_4F_8 flow rates: (a) F/C ratio from the CVD ACL surface at a fixed CF_4 flow rate of 50 SCCM, (b) F/C ratio from the SiCOH surface at a fixed CF_4 flow rate of 50 SCCM, and (c) Si/O ratio from the SiCOH at a fixed CF_4 flow rate of 50 SCCM.

face, which indicates the formation of a more F-deficient CH_xF_y layer on the SiCOH surface. These results indicate that fluorine atoms in the CH_xF_y polymer on the SiCOH surface are consumed more effectively compared to the case of ACL, which leads to a more F-deficient CH_xF_y polymer layer. Chemical reactions between fluorine in the the CH_xF_y polymer and silicon in the SiOCH layer can lead to effective consumption of fluorine in the CH_xF_y polymer and, in turn, to a decrease the F/C ratio. Figure 5(c) shows the variation of Si/O ratio on the SiCOH layer with the C_4F_8 flow rate. The Si/O ratio increased as the C_4F_8 flow rate was increased. As the C_4F_8 flow rate was increased, oxygen atoms in the SiCOH can be effectively removed due to formation of CO, CO_2, and COF_2 by-products, thus increasing the Si/O ratio.

In order to confirm the CH_xF_y layer formation on the SiCOH surface with increasing C_4F_8 flow rate, we measured the thickness of the hydrofluorocarbon layer ($d_{CH_xF_y}$), on SiCOH. The CH_xF_y on ACL cannot be determined using XPS spectra due to the existence of carbon in the ACL. Due to this problem, the $d_{CH_xF_y}$ estimated from the the CH_xF_y layer deposited on Si was referenced even though the $d_{CH_xF_y}$ on ACL is expected not to be the same as that on Si. From the patterned samples, the $d_{CH_xF_y}$ on ACL was found to be slightly larger than the $d_{CH_xF_y}$ on Si. Figure 6 shows the $d_{CH_xF_y}$ values on the Si wafer determined from the C 1s spectra as a function of the C_4F_8 flow rate. The method used to calculate the $d_{CH_xF_y}$ on the SiCOH and on the Si surface is essentially the same as that outlined in other reports [17–19]. The d_{CHxFy} values were calculated from the integrated C 1s photoemission intensities ($I^d_{C(1s)}$) by using the C 1s reference intensity ($I_{C(1s)}$) of the passively-deposited thick CH_xF_y layer on Si substrate, where $\lambda_{C(1s)}$ are the electron mean free paths of

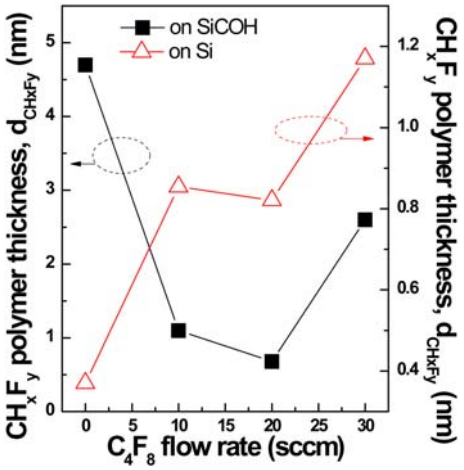

Fig. 6. (Color online) Steady-state thickness of the CH_xF_y layer, $d_{CH_xF_y}$, calculated from the C 1s XPS spectra of the etched CVD ACL and the SiCOH as functions of the C_4F_8 flow rate at a fixed CF_4 flow rate of 50 SCCM.

the C 1s photoelectrons. For our calculations, $\lambda_{C(1s)}$ was set to 2.5 nm [17,19-21].

As shown in Fig. 6, the $d_{CH_xF_y}$ on the SiCOH decreased with increasing C_4F_8 flow rate from 0 to 20 SCCM, which is opposite to the case of CH_xF_y deposition on Si. The tendency of CH_xF_y deposition thickness on the ACL is expected to be similar to that on Si due to decreased elemental O in the ACL. Even with an increase in the polymerizing C_4F_8 gas, there is an effective reaction of C and F species in the CH_xF_y polymer with elemental O and Si in the SiCOH, respectively. However, the $d_{CH_xF_y}$ on the SiCOH increased at a C_4F_8 flow rate of 30 SCCM due to high polymerization at a high C_4F_8 flow rate. Therefore, a disproportionate formation of a

CH_xF_y layer on the ACL and the SiCOH surfaces can result in a process window for ultra-high etch selectivity between the ACL and the SiCOH layers. In addition, the formation of F-rich, thinner CH_xF_y polymers on the SiCOH surface with the addition of C_4F_8 is attributed to the observed increases in the CD (Fig. 2(a)) and the LER (Fig. 2(b)).

IV. CONCLUSION

In this work, we used a DFS-CCP etcher to investigate the effects of C_4F_8 flow rate on the etch rates of SiCOH and ACL, the etch selectivity of SiCOH layer to ACL, and the variation of the CD size and the LER in $CF_4/C_4F_8/Ar$ plasmas. The process region for ultra-high SiCOH/ACL etch selectivity could be obtained under a certain flow region of the C_4F_8 gas. The results indicate that the flow rate of the C_4F_8 gas is a crucial parameter because it controls the thickness of the steady-state CH_xF_y layer on the SiCOH surface, as well as the net deposition of the CH_xF_x layer on the ACL. For polymerizing etch chemistry with very high etch selectivity, variations in the CD size and the LER of the etched patterns were also observed. Therefore, optimization of the process conditions is needed if the present experimental results are to be applied to practical nano-scale etch applications utilizing a very thin ACL hard-mask during Si chip fabrication.

ACKNOWLEDGMENTS

This work was supported by the "Development Program of Nano Process Equipments" of the Ministry of Knowledge Economy [10034827, Development of 450 mm plasma technology for low-damage nano-device processes]. This research was also partially supported by the Ministry of Knowledge Economy (MKE) and Korea Industrial Technology Foundation (KOTEF) through the Human Resource Training Project for Strategic Technology.

REFERENCES

[1] R. M. Badam, M. M. Roy, W. Shaoyu and A. Naman, Jpn. J. Appl. Phys. **43**, 7381 (2004).
[2] H. Nagai, S. Takashima, M. Hiramatsu, M. Hori and T. Goto, J. Appl. Phys. **91**, 2615 (2002).
[3] H. Cui, R. J. Carter, D. L. Moore, Hua-Gen Peng, D. W. Gidley and P. A. Burke, J. Appl. Phys. **97**, 113302 (2005).
[4] S. K. Yang *et al.*, J. Korean Phys. Soc. **52**, 1786 (2008).
[5] H. T. Kim, B. S. Kwon, N-E. Lee, Y. S. Park, H. J. Cho and B. Hong, J. Vac. Sci. Technol. A **26**, 861 (2008).
[6] V. Constantoudis, G. Kokkoris, P. Xydi, G. P. Patsis and E. Gogolides, Microelectron. Eng. **86**, 968 (2009).
[7] D. L. Goldfarb *et al.*, J. Vac. Sci. Technol., B **22**, 647 (2004).
[8] D. H. Kim, S. H. Cho, N-E. Lee and K. C. Kwon, Jpn. J. Appl. Phys. **44**, 5856 (2005).
[9] D. H. Kim, C. H. Lee, S. H. Cho and N.-E. Lee, J. Vac. Sci. Technol. B **23**, 2203 (2005).
[10] A. Kojima *et al.*, in *Proc. Dry Process Int. Symp.* (Tokyo, Japan, 2003), p. 13.
[11] J. Robiche, P. C. Boyle, M. M. Turner and A. R. Ellingboe, J. Phys. D: Appl. Phys. **36**, 1810 (2003).
[12] M. H. Jeon, S-K. Kang, J. Y. Park and G. Y. Yeom, J. Korean Phys. Soc. **59**, 3024 (2011)
[13] B. S. Kwon, J. S. Kim, N.-E. Lee, S. K. Lee and S. W. Park, J. Korean Phys. Soc. **58**, 1622 (2011)
[14] V. Georgieva, A. Bogaerts and R. Gijbels, J. Appl. Phys. **94**, 3748 (2003).
[15] C. Cardinaud, A. Rhounna, G. Turban and B. Grolleau, Rev. Phys. Appl. **24**, 309 (1989).
[16] T. Shirasaki, F. Moguet, L. Lozano, A. Tressaud, G. Nase and E. Papirer, Carbon **37**, 1891 (1999).
[17] J. Chastain and R. C. King Jr., *Handbook of X-ray Photoelectron Spectroscopy* (Physical Electronics Inc., Eden Prairie, USA, 1995).
[18] Y. Zhang, G. S. Oehrlein and F. H. Bell, J. Vac. Sci. Technol., A **14**, 2127 (1996).
[19] T. E. F. M. Standaert, C. Hedlund, E. A. Joseph, G. S. Oehrlein and T. J. Daltone, J. Vac. Sci. Technol., A **22**, 53 (2004).
[20] C. K. Park, H. T. Kim, C. H. Lee, N. E. Lee and H. Mok, Microelectron. Eng. **85**, 375 (2008).
[21] D. Briggs and M. P. Seah, *Practical Surface Analysis*, 2nd ed. (Wiley, New York, 1990), Vol. 1.